Published as: C. Demirci, C. Málaga-Chuquitaype and L. Macorini. (2019) "Shear and acceleration demands in multi-storey cross-laminated timber buildings." Engineering Structures. https://doi.org/10.1016/j.engstruct.2019.109467
BibTeX:
@article{cagatay2019shear,
title={Shear and acceleration demands in multi-storey cross-laminated timber buildings},
author={Demirci, Cagatay and M{\'a}laga-Chuquitaype, Christian and Macorini, Lorenzo},
journal={Engineering Structures},
year={2019},
doi={10.1016/j.engstruct.2019.109467}
publisher={Elsevier}}

Seismic shear and acceleration demands in multi-storey cross-laminated timber buildings

Cagatay Demirci[a], Christian Málaga-Chuquitaype[a,*], Lorenzo Macorini[a]

[a]*Department of Civil and Environmental Engineering, Imperial College London, UK*

Abstract

A realistic estimation of seismic shear demands is essential for the design and assessment of multi-storey buildings and for ensuring the activation of ductile failure modes during strong ground-motion. Likewise, the evaluation of seismic floor accelerations is fundamental to the appraisal of damage to non-structural elements and building contents. Given the relative novelty of tall timber buildings and their increasing popularity, a rigorous evaluation of their shear and acceleration demands is all the more critical and timely. For this purpose, this paper investigates the scaling of seismic shear and acceleration demands in multi-storey cross-laminated timber (CLT) buildings and its dependency on various structural properties. Special attention is given to the influence of the frequency content of the ground-motion. A set of 60 CLT buildings of varying heights representative of a wide range of structural configurations is subjected to a large dataset of 1656 real earthquake records. It is demonstrated that the mean period (T_m) of the ground-motion together with salient structural parameters such as building aspect ratio (λ), design force reduction factor (q) and panel subdivision (β) influence strongly the variation of base shear, storey shears and acceleration demands. Besides, robust regression models are used to assess and quantify the distribution of force and acceleration demands on CLT buildings. Finally, practical expressions for the estimation of base shears, inter-storey shears and peak floor accelerations are offered.

Keywords: cross-laminated timber, shear demands, peak acceleration, ground-motion frequency content, mean period, tall timber buildings

1. Introduction

Multi-storey wooden buildings with lateral resisting systems formed of cross-laminated timber (CLT) panels are being increasingly used in earthquake prone regions. The rise in the popularity of wooden buildings obeys to the numerous benefits offered by timber structural systems in comparison with their more traditional counterparts in steel and concrete. Timber comparative advantages include its minimum carbon footprint, outstanding structural efficiency and reduced erection time and cost. In addition, CLT panellized construction displays high dimensional stability and allows large-scale prefabrication.

The dynamic response of CLT buildings under earthquake loading has been the subject of numerous experimental and numerical studies over the last two decades. Among others, the SOFIE project [1] stands out as one of the most comprehensive experimental investigations on the seismic behaviour of CLT buildings. Carried out by CNR-IVALSA, it involved testing a large number of shear-walls and various joint arrangements together with shaking-table experimentation on full-scale 3- and 7-storey CLT building specimens [1, 2]. It was observed that, while CLT panels behave rigidly, the seismic energy dissipation capacity of the connections and their stiffness are the main factors influencing the overall response of CLT structures.

*Corresponding author
Email address: c.malaga@imperial.ac.uk (Christian Málaga-Chuquitaype)

Other experimental research efforts to assess the lateral response of CLT buildings and panels are reported in [3, 4, 5, 6, 7, 8, 9, 10]. In general, a relatively good and ductile seismic response was observed in CLT structures that are appropriately designed and assembled. The role of connector ductility, joint capacity, panel arrangement, wall aspect ratio and level of vertical loads on the seismic behaviour of CLT walls and assemblages has also been recognised.

A large number of numerical studies on the seismic behavior of CLT buildings have also been performed [8, 11, 12, 13, 14, 15, 16]. However, the vast majority of these research efforts have been limited to the calibration of FE models against experimental results, and the identification of adequate response modification factors for low and mid-rise CLT buildings. Pei *et al.* [14] suggested the use of a seismic response modification factor, R, of 4.5 based on numerical analyses on a six-storey CLT building designed following American procedures [17]. On the other hand, a seismic force reduction factor, q, of 3.0 was recommended by Sustersic *et al.* [18] based on response-history analyses performed as part of the SOFIE project. Similarly, Fragiacomo *et al.* [13], carried out a numerical investigation to determine behaviour factors, q, within the context of European design provisions [19]. More recently, the inelastic deformation demands in multi-storey CLT structures were studied by Demirci *et al.* [20] by employing an extensive database of CLT buildings and real earthquake accelerograms. Their study highlighted the crucial role played by the ground-motion frequency content on the evolution of inelastic deformations in timber buildings. Nevertheless, to date, no comprehensive assessment has been conducted on the distribution of strength (shear) and acceleration demands in CLT buildings where the influence of higher modes and ground-motion frequency content is expected to be determinant [21]. Moreover, generalizable performance-based design inferences for CLT buildings are sorely needed.

Following the previous discussion, this paper seeks to offer a comprehensive characterization of global and storey strength demands as well as peak floor accelerations in multi-storey CLT buildings. The influence of the mean period of the ground-motion, T_m, on maximum forces and accelerations is rigorously assessed by analysing the response of 60 CLT buildings, from 6 to 20 storeys in height, subjected to a large set of real ground-motions. Following a detailed description of the numerical models and ground-motion database employed, the paper continues with a complete assessment of their associated seismic demands and underlying tendencies. Finally, predictive models for the estimation of shear forces and floor accelerations are formulated.

2. Building database and modelling

2.1. Seismic design

In order to represent a wide range of structural configurations, a total of 60 cross-laminated timber buildings were designed in accordance with accepted scientific knowledge and ductile design principles. Capacity design considerations and failure mode control, as outlined in Eurocode 8 and applied in common design practice, were followed in this study [22]. An overview of the general principles of seismic design of timber structures within European practice can be found in [19].

A typical plan view and the elevation of a 6-storey CLT building are depicted in Figure 1 based on an 8-storey building designed by Málaga-Chuquitaype [23]. The same plan layout was employed for all buildings considered in this paper. The building layout includes a podium at the ground level (detached from the structural walls) and the number of stories of the tower block, n, was varied between 6 and 20 at regular intervals (i.e. $n = \{6, 8, 12, 16, 20\}$). The adopted structural system comprises CLT shear walls in both X and Y directions as illustrated in Figure 1. Only the 2D response of a wall along the X-axis (wall 2-BC in Figure 1) is considered in the present study. 5-layered CLT panels ranging from 95 mm thickness (19-19-19-19-19) to 200 mm (40-40-40-40-40) were employed. Similarly, roof and floor slabs made of 5-layered CLT panels of 200 mm thickness were considred in all buildings. All panel thicknesses were selected to satisfy ultimate and serviceability limit states verifications considering vertical and horizontal loads as well

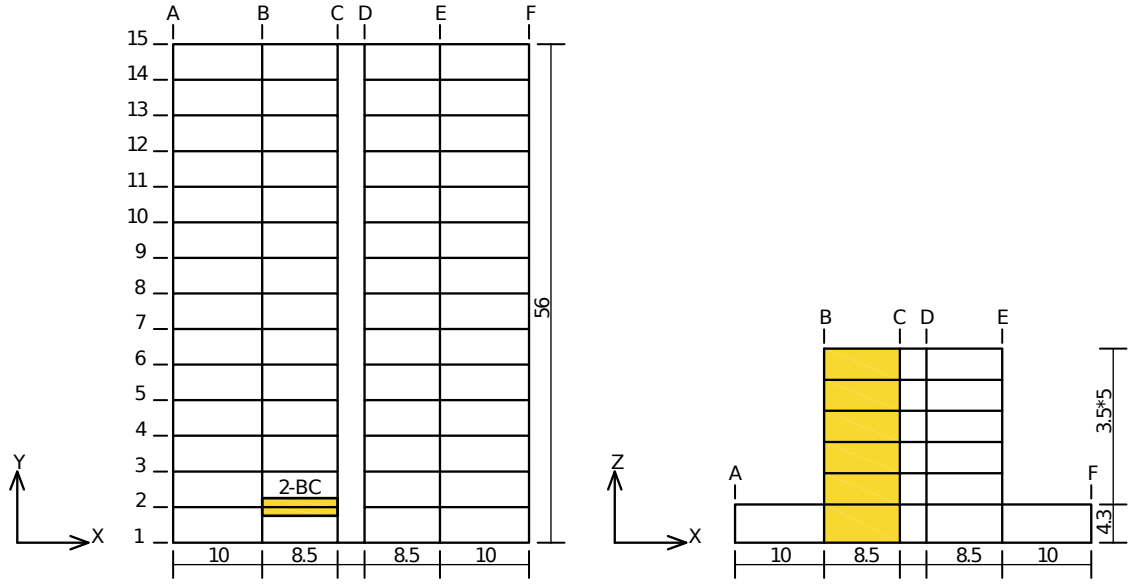

Figure 1: Plan view and the elevation of a typical 6-storey CLT building. Wall 2-BC, shown yellow in the figure, is selected for subsequent analyses. Units in [m].

as load combinations and capacity design considerations. Class C24 timber (according to BS 25 EN 14081-1: 2005 [24]) was adopted for all CLT panels. Nominal design material properties where obtained from their corresponding characteristic values following the directives of Eurocode 8 for seismic scenarios [19, 25].

Dead loads were calculated taking into account all finishings and insulation whereas a live load of 2.00 kN/m^2 (Service Class A) was considered for the floors and the roof [26, 25]. A combination of the dead load plus 30% of the total superimposed load was assumed for seismic assessment purposes. Table 1 summarizes typical loads and seismic masses employed for the 6-storey CLT building as an example. Similarly, the Eurocode Type 1 Response Spectrum (for seismic prone areas) was employed together with soil type C conditions [25] and a reference peak ground acceleration of 3 m/s^2.

Failure mode control principles were employed and the number of hold-down and shear connectors at each level was calculated accordingly. Two HBS 8x80 mm self-drilling screws per row were used at the spline step joints with average spacing between 40 and 80 mm at the ground level, depending on capacity design requirements [27, 28, 29]. Also, the spacing between screws was reduced at upper levels in proportion to the magnitude of forces acting on the joints. The capacity design principles outlined in [30] which try to enforce regularity in elevation were employed to this effect. The main structural characteristics of the set of prototypical buildings designed as described above are summarized in Table 2. This table also includes the number and type of shear brackets and tension hold-downs [31] employed per panel at the bottom storey. As with step-joints, the number of shear brackets and hold-downs also reduces at higher levels in direct proportion to the storey shears. As an example, Table 3 presents the variation of connector configuration for the 6-storey building (A1). Besides, it is necessary to ensure an adequate failure mode where energy dissipation happens through controlled yielding at the metallic connectors and other parts of the structure are designed with enough over strength to avoid premature failure. The connections that were over-designed were: connections between floors and the walls underneath, connections between floor panels that form the rigid diaphragm, and connections between perpendicular walls. 5x50 mm LBS screws are employed in all hold down connectors (20 screws for WHT340, 30 for WHT440, 45 for WHT540 and 55 for WHT620) [31]. On the other hand, 30 LBA nails of 4x60 mm are employed for the angle bracket type TTF200 per flange [31].

Table 1: Summary of loads and seismic massess in the 6-storey building.

Level	Dead load [kN]	Superimposed load [kN]	Seismic mass [Tonnes]
Ground	8878.4	7260	1127.4
2	5313.5	2780	626.9
3	5313.5	2780	626.9
4	5313.5	2780	626.9
5	5313.5	2780	626.9
6	4365.8	2240	513.7
Total	34498	20620	4149

2.2. Main structural characteristics

Advanced finite elements models were constructed, as described in the following section, and eigenvalue and non-linear static pushover analyses were performed to obtain some of the parameters presented in Table 2. The main characteristics of the multi-storey CLT buildings considered in this study are:

- Behaviour factor, q. Although the use of a behaviour factor of $q = 3$ is recommended by a number of researchers [12, 32, 33, 19], in this study q factors of $q = \{2, 2.5, 3, 4\}$ were employed to encompass a wider range of design assumptions and practices as presented in Figure 2.

- Number of vertical joint lines, m, which quantifies the level of panel fragmentation assumed in the design of the CLT buildings. m values of $m = \{1, 2, 3\}$ were adopted in the present study.

- Fundamental period, T_1, which was obtained from eigenvalue analyses on the numerical models described below. Figure 2a shows the distribution of fundamental periods of the set of buildings employed. These periods range from 0.3 s for the shorter structures to 1.0 s for the taller ones.

- Building aspect ratio or slenderness, λ. The slenderness of the building is calculated as the ratio between the height and the width of its facade. Figure 2b presents the distribution of building aspect ratios employed with values varying from 2.56 to 8.33.

- Joint density parameter, β, which is defined in [34] as the ratio between all fastening lines in the wall, P_0, against the perimeter of the wall, P. The distribution of β for the dataset of building employed in this study is presented in Figure 2c.

- Plasticity resistance ratio, α, that, following other sections of Eurocode 8 [25], is defined as the ratio between the ultimate base shear, V_u, when a plastic mechanism is developed in the structure, and the base shear at yield, V_1 . The distribution of the plasticity resistance ratios of the population of buildings considered herein is shown in Figure 2d and ranges from 1.8 to 3.8.

It is important to understand the correlation among the structural characteristics of the building dataset created. For this purpose, Figure 3 presents a scatter plot matrix of the fundamental period (T_1), the plasticity resistance ratio (α), the joint density parameter (β), and the building aspect ratio (λ). The lower panels in this figure show the distribution of the key structural parameters shown in the diagonal with a trend line obtained by means of a locally weighted regression. The associated histograms are presented in the diagonal boxes while the upper panels present the p-values and correlation coefficients for each trendline identified. The scatter plot presented in Figure 3 informed the development of the predictive models presented later in this paper.

Table 2: Structural characteristics of prototypical buildings designed with a behaviour factor of $q = 3$.

Storeys	$n = 6$			$n = 8$			$n = 12$			$n = 16$			$n = 20$		
ID	A1	A2	A3	B1	B2	B3	C1	C2	C3	D1	D2	D3	E1	E2	E3
Vertical joint line	$m = 1$	$m = 2$	$m = 3$	$m = 1$	$m = 2$	$m = 3$	$m = 1$	$m = 2$	$m = 3$	$m = 1$	$m = 2$	$m = 3$	$m = 1$	$m = 2$	$m = 3$
T_1 [s]	0.360	0.349	0.340	0.431	0.425	0.414	0.618	0.616	0.581	0.816	0.839	0.878	0.951	1.039	0.914
α	3.838	2.237	1.911	2.748	2.261	1.819	2.442	2.184	2.046	3.510	2.1984	1.9402	3.617	2.275	2.527
CLT panel thickness in [mm]	125 (1-3) 95 (4-6)	125 (1-3) 95 (4-6)	125 (1-3) 95 (4-6)	125 (1-3) 95 (4-8)	125 (1-3) 95 (4-8)	125 (1-3) 95 (4-8)	140 (1-3) 125 (4-8) 95 (9-12)	140 (1-3) 125 (4-8) 95 (9-12)	140 (1-3) 125 (4-8) 95 (9-12)	180 (1-3) 140 (4-6) 125 (8-16)	180 (1-3) 140 (4-6) 125 (8-16)	180 (1-3) 140 (4-6) 125 (8-16)	200 (1-3) 140 (4-6) 125 (8-20)	200 (1-3) 140 (4-6) 125 (8-20)	200 (1-3) 140 (4-6) 125 (8-20)
Shear brackets per panel	6 TTF 200	4 TTF 200	3 TTF 200	8 TTF 200	5 TTF 200	4 TTF 200	9 TTF 200	6 TTF 200	5 TTF 200	10 TTF 200	7 TTF 200	5 TTF 200	10 TTF 200	7 TTF 200	5 TTF 200
Tension brackets per panel	4 WHT 620	2 WHT 620	2 WHT 620	2 WHT 620	2 WHT 620	2 WHT 620	4 WHT 620	4 WHT 620	4 WHT 620	4 WHT 620	4 WHT 620	4 WHT 620	4 WHT 620	4 WHT 620	4 WHT 620

Table 3: Variation of the number of metal connectors in Building A1.

Level	$q = 2$	$q = 2.5$	$q = 3$	$q = 4$
1	9 TTF200 4 WHT620	8 TTF200 4 WHT620	6 TTF200 4 WHT620	5 TTF200 2 WHT620
2	9 TTF200 4 WHT620	7 TTF200 4 WHT620	6 TTF200 2 WHT620	5 TTF200 2 WHT620
3	8 TTF200 4 WHT540	6 TTF200 4 WHT540	5 TTF200 2 WHT540	4 TTF200 2 WHT540
4	6 TTF200 4 WHT440	5 TTF200 4 WHT440	4 TTF200 2 WHT440	3 TTF200 2 WHT440
5	5 TTF200 4 WHT440	4 TTF200 2 WHT440	3 TTF200 2 WHT440	3 TTF200 2 WHT440
6	3 TTF200 2 WHT340	3 TTF200 2 WHT340	3 TTF200 2 WHT340	3 TTF200 1 WHT340

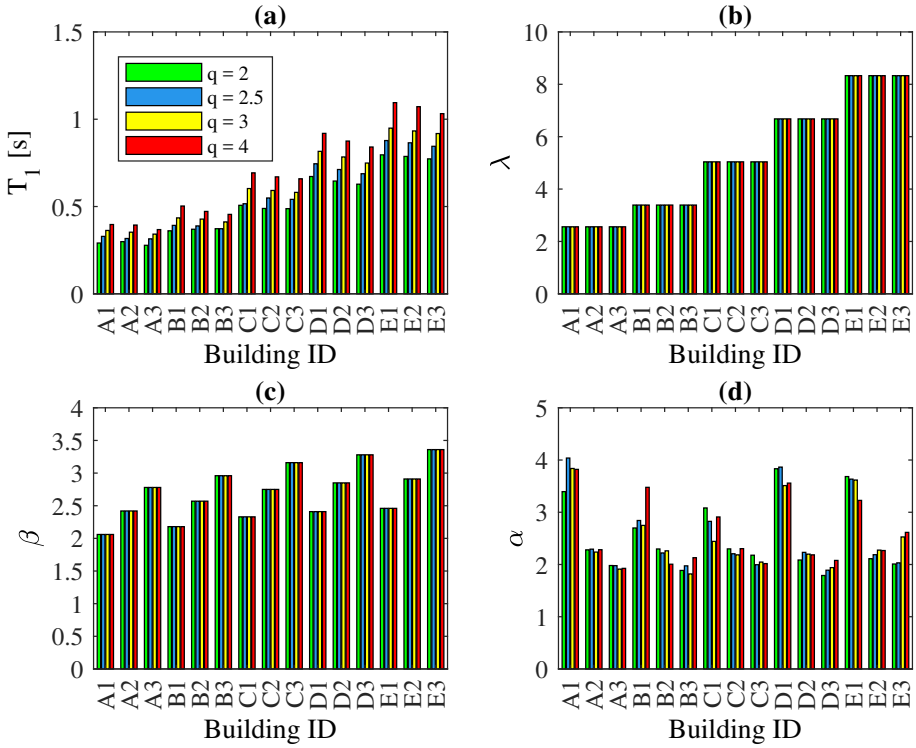

Figure 2: Distributions of structural properties of the buildings employed in this study plotted with respect to different design practices, $q = \{2, 2.5, 3, 4\}$.

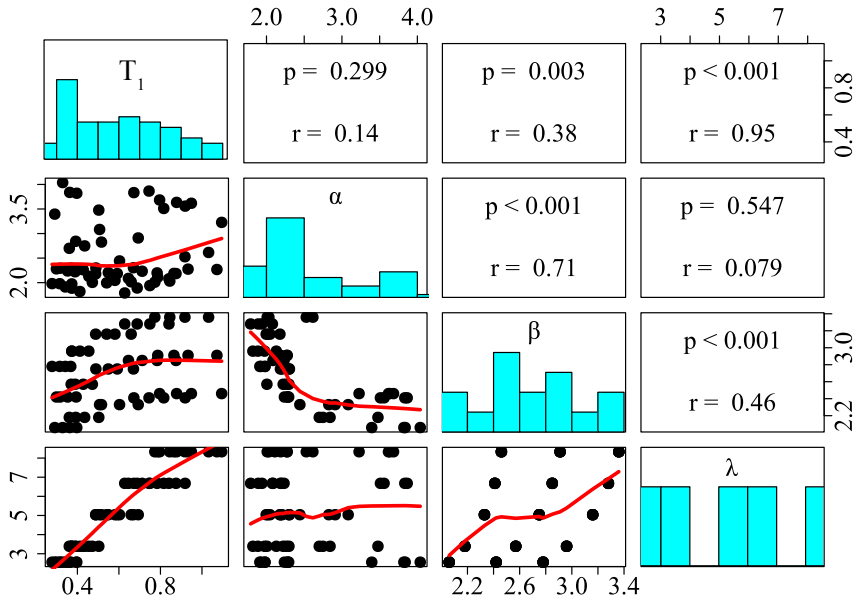

Figure 3: Scatterplot matrix of the key structural characteristics. Generated in R [35, 36].

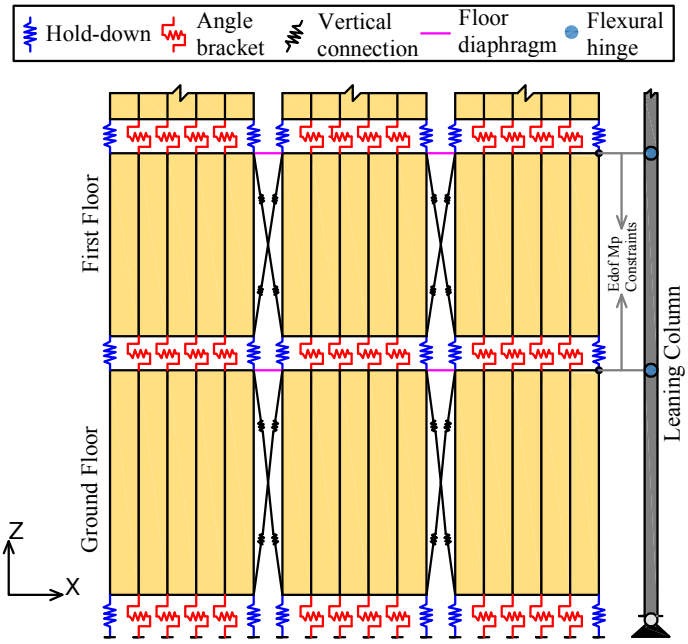

Figure 4: Numerical modelling approach for CLT buildings.

2.3. Numerical modelling approach

Numerical models of the CLT core sections of the buildings described above were developed in the Finite Element framework OpenSees [37]. Figure 4 depicts the numerical modelling approach adopted. It is common practice in modelling of CLT structures to concentrate the non-linear deformations at the connectors. Thus, linear-elastic 4-node *Quad* elements available in OpenSees [37] were employed to simulate the CLT panels whereas 3-linear hysteretic models were adopted for the connectors. Following preliminary investigations on the influence of orthotropic material modelling and vertical loads on the performance of CLT numerical models [20], an equivalent isotropic wood material model was employed for the load-bearing CLT panels.

It is worth noting that the implementation of 4-node *Quad* elements in OpenSees [37] relies on a 2-degree-of-freedom per-node idealization with purely linear geometric transformation. Therefore, in order to account for second order P-delta effects, a leaning column was attached to the CLT shear-wall as schematically shown in Figure 4. The leaning column was constructed employing pin-jointed elastic beam-column elements with 3-degrees-of-freedom per-node and a *Co-rotational* geometric transformation. The corresponding vertical loads were applied on the leaning column at each storey level. An Equal Degree-of-Freedom (*EdofMP*) multi-point constraint connecting the CLT shear-wall and the idealized leaning column was used to simulate the rigid diaphragm action. Zero-length and two-node link elements with *Hysteretic* material model [37] were employed to simulate shear brackets, tie-down connectors and the structural joinery between adjacent CLT wall panels considering un-coupled hysteretic behaviour in the two perpendicular directions. Therefore, tension and shear forces interaction was not explicitly accounted for and the interested reader is referred to other works [38] for instances of its implementation. A careful calibration process againts available experimental data [31, 39, 40] was carried out in order to define adequate stiffness and strength degradation parameters for the hysteretic models. To this end, stiffness and strength degradation factors between 0.2 and 0.8 [37] were found to provide a very close estimation of the full hysteretic response of the joints [20, 22].

2.4. Numerical model validation

Extensive numerical validation studies have been performed to verify the numerical modeling strategy adopted. Available experimental results [39] on shear and a tension connectors, single CLT walls, coupled CLT panels as well as a multi-storey building [16] were employed for these validations. To this end, Figure 5 presents the calibration of non-linear springs to a BMF 90x48x3x116 mm angle bracket and a HTT22 [31] hold-down connector. A more comprehensive description of the numerical and experimental comparisons can be found in [20, 22]. Only selected results corresponding to the simulation of the experimental response of the 7-storey SOFIE building are presented herein. For this purpose, the plan view of the experimental specimen [16] is depicted in Figure 6a while Figure 6b shows a schematic representation of the OpenSees model. The predictions of a 2D response corresponding to the Y-direction of the building are compared below against the response of the full-scale 3D building subjected to multi-axial earthquake excitation. Further details of the specimen configurations and experimental campaign can be found in [16].

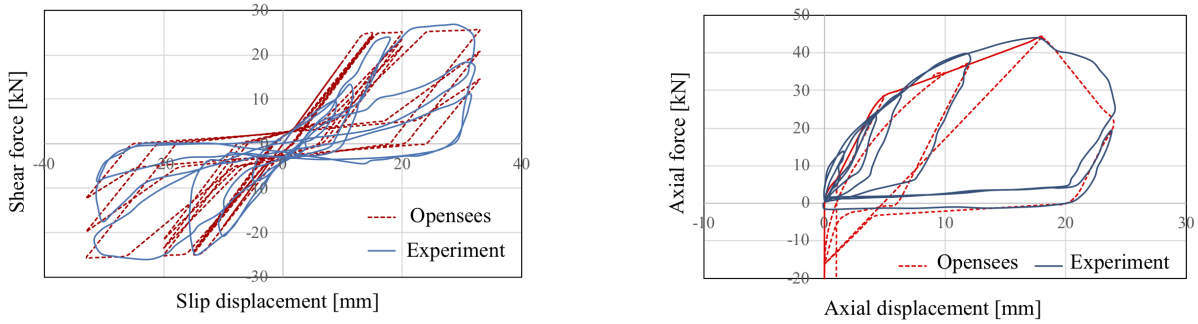

(a) Shear bracket. (b) Hold-down.

Figure 5: Calibration of non-linear springs representing the experimental response [39, 40] of metal connectors.

Figure 7 compares the observed experimental response and FE model predictions. The displacement histories presented in Figures 7a and 7b correspond to the first and top levels of the building, respectively. Likewise, the numerical and experimental acceleration responses at the top floor are compared in Figure 7c. Furthermore, an evaluation in terms of cumulative energy dissipation is presented in Figure 7d, where a maximum difference of less than 7% is observed. These results support the use of the the numerical modelling approach described in the previous section. It is clear that, despite the simplifications involved in the numerical representation, a good agreement is found between the measured structural response and the numerical model estimations.

3. Ground motion records and frequency content

A total of 1656 real ground-motion records coming from 51 seismic events with Moment magnitudes, M_w, between 5.1 and 7.9 and an average peak ground accelertion of 1 g were employed. The dataset comprises acceleration histories collected at distances, R_{jb}, from 1 to 200 km of which 17% were recorded in rock sites, 42% in stiff soils and 41% in soft soil conditions coming from the PEER-NGA database. The catalogue of earthquakes employed in the study is presented in Table 4 below. Additional information on the ground-motion database can be found in [20, 41].

The frequency content of the ground motion is characterized in this study by means of the mean period, T_m. The mean period was initially proposed by Rathje *et al.* [42, 43] and has been identified as a good indicator of the frequency content of a ground-motion leading to improved estimates of peak structural

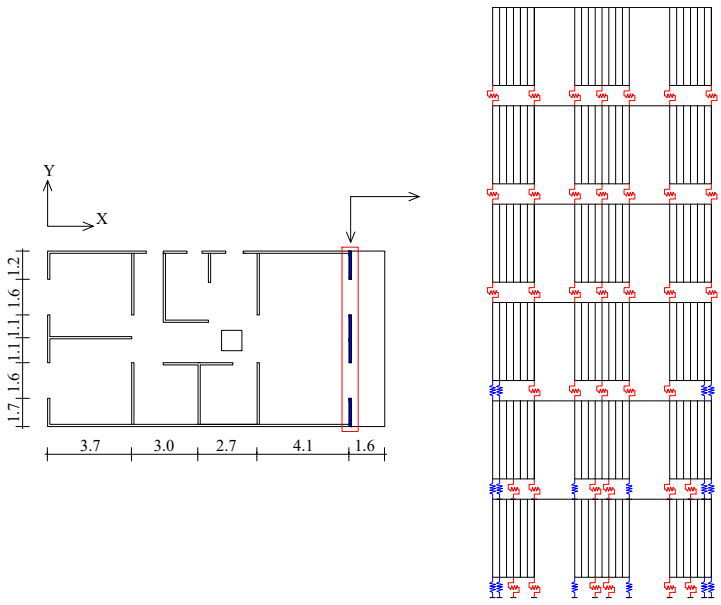

(a) Typical floor plan. (b) Numerical model.

Figure 6: Plan view and the elevation of OpenSees model of the SOFIE building.

deformations [44, 45, 46]. It is calculated as the weighted mean, over a pre-defined frequency range, of the corresponding periods ($\frac{1}{f_i}$) in the Fourier Spectrum:

$$T_m = \frac{\Sigma_i C_i^2 \cdot \frac{1}{f_i}}{\Sigma_i C_i^2} \quad for \;\; 0.25\ Hz \leq f_i \leq 20\ Hz \;\; with \;\; \Delta f \leq 0.05\ Hz \tag{1}$$

where C_i is the Fourier amplitude corresponding to ith frequency, f_i, and Δf is the spacing between the frequencies.

4. Assessment of seismic shear demands

4.1. Assessment procedure

More than 100 000 analyses were performed using the paralellized FE tool OpenSeesMP at Imperial College Research Computing Service [47]. The results were subsequently post-processed in order to identify maximum base shear, V_{max}, and maximum inter-storey shear, $V_{i,max}$, forces as well as peak floor accelerations, a_{max}. This section will focus on base shear and inter-storey shear demands, while the next section will discuss the results obtained for acceleration amplification factors. To this end, the following shear force modification factors are of interest:

- *Base shear modification factor*, V_{mod}, is the ratio between the maximum base shear, V_{max}, obtained from the non-linear response history analysis and the product of the plasticity resistance ratio, α, times the base shear at yield, V_1. The base shear at yield is calculated as the sum of all the ground-level connector forces at the point of first yield, and is obtained from a non-linear static analysis with monotonically increasing lateral loads adopting a first mode distribution along the building's height. V_{mod} can be expressed as:

$$V_{mod} = \frac{V_{max}}{\alpha \cdot V_1} \tag{2}$$

Table 4: Ground motion catalogue employed.

EQ No	EQ name	Year	Moment magnitude (Mw)	Number of records
1	Imperial Valley-02	1940	6.95	2
2	Kern County	1952	7.36	4
3	Parkfield	1966	6.19	11
4	Borrego Mtn	1968	6.63	8
5	San Fernando	1971	6.61	54
6	Managua, Nicaragua-01	1972	6.24	2
7	Friuli, Italy-01	1976	6.5	8
8	Gazli, USSR	1976	6.8	2
9	Friuli, Italy-02	1976	5.91	4
10	Santa Barbara	1978	5.92	4
11	Tabas, Iran	1978	7.35	14
12	Coyote Lake	1979	5.74	18
13	Imperial Valley-06	1979	6.53	68
14	Mammoth Lakes-01	1980	6.06	4
15	Victoria, Mexico	1980	6.33	9
16	Irpina, Italy-01	1980	6.9	20
17	Irpina, Italy-02	1980	6.2	14
18	Corinth, Greece	1981	6.6	2
19	Westmorland	1981	5.9	8
20	Coalinga-01	1983	6.36	86
21	Borah Peak, ID-01	1983	6.88	12
22	Morgan Hill	1984	6.19	49
23	Lazio-Abruzzo, Italy	1984	5.8	2
24	Nahanni, Canada	1985	6.76	6
25	N. Palm Springs	1986	6.06	22
26	Chalfant Valley-01	1986	5.77	8
27	Chalfant Valley-02	1986	6.19	16
28	San Salvador	1986	5.8	4
29	Whittier Narrows-01	1987	5.99	81
30	Superstition Hills-01	1987	6.22	2
31	Superstition Hills-02	1987	6.54	22
32	Loma Prieta	1989	6.93	163
33	Erzincan, Turkey	1992	6.69	2
34	Cape Mendocino	1992	7.01	10
35	Landers	1992	7.28	130
36	Northridge-01	1994	6.69	296
37	Kobe, Japan	1995	6.9	44
38	Kozani, Greece-01	1995	6.4	2
39	Dinar, Turkey	1995	6.4	8
40	Gulf of Aqaba	1995	7.2	4
41	Kocaeli, Turkey	1999	7.51	55
42	Duzce, Turkey	1999	7.14	44
43	Sitka, Alaska	1972	7.68	4
44	Caldiran, Turkey	1976	7.21	2
45	St Elias, Alaska	1979	7.54	4
46	Manjil, Iran	1990	7.37	15
47	Sierra, Madre	1991	5.61	4
48	Little Skull Mtn, NV	1994	5.65	16
49	Hector Mine	1999	7.13	167
50	Nenana Mountain, Alaska	2002	6.7	72
51	Denali, Alaska	2002	7.9	48
Total number of records				1656

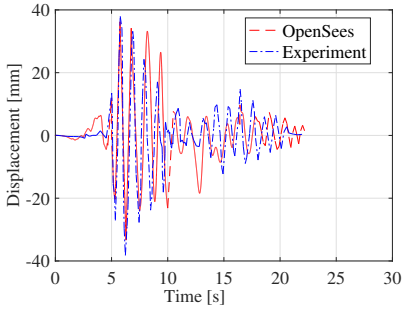

(a) Experimental [16] and numerical displacement histories at the 1st level.

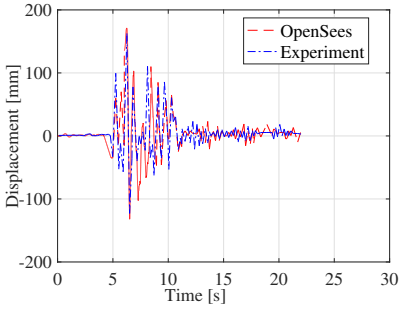

(b) Experimental [16] and numerical displacement histories at the top level.

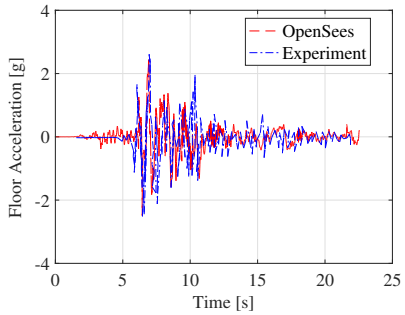

(c) Experimental [16] and numerical acceleration histories at the top level.

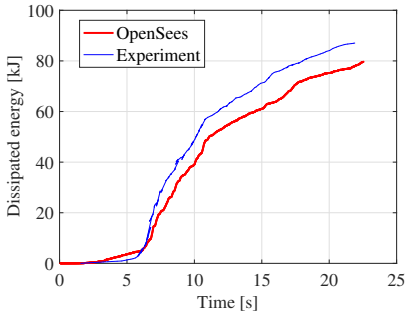

(d) Experimental and numerical comparison of cumulative dissipated energy.

Figure 7: Experimental [16] and numerical comparison of the response of SOFIE building.

- *Inter-storey shear modification factor*, $V_{st,mod}$, is the ratio between the maximum inter-storey shear at the i-th storey of the building, $V_{i,max}$, obtained from non-linear response history analysis and the product of the plasticity resistance ratio, α, times the total inter-storey shear at the i-th storey at yield, $V_{i,1}$. The storey shear at yield, $V_{i,1}$, is calculated as the sum of the shear forces in all shear walls of the storey being considered at the point of first yield. $V_{st,mod}$ is defined as:

$$V_{st,mod} = \frac{V_{i,max}}{\alpha \cdot V_{i,1}} \tag{3}$$

It should be noted that the definitions offered above follow widely accepted formulations for structures dimensioned according to ductile design approaches [25, 48]. In the following sections, the results of the large dataset of non-linear static and dynamic analyses created are examined to investigate the influence of various structural characteristics on base and inter-storey shear modification factors.

4.2. Base shear demands

The variation of base shear modification factors, V_{mod}, for the A1 (n = 6) building configuration as a function of the period ratio, T_1/T_m, is presented in Figure 8a whereas Figure 8b shows the corresponding results for the E1 (n = 20) building. The period ratio, is defined as the ratio between the fundamental period of the structure (T_1) and the mean period of the ground-motion (T_m) while the base shear modification factor is defined as explained above. The open circles (o) and asterisks (*) symbols in Figure 8 denote the mean and median values within each data bin, respectively. The shaded regions show the 95% confidence interval in the estimate of the mean base shear and the dotted lines depict the ± one standard deviation limits of the base shear modification factor, lnV_{mod}, for the best-fit prediction model described in latter parts of this

paper. The mean estimate of the best-fit prediction model is depicted by the solid line in Figure 8. Plots like these have long been employed to assess the fitting ability of regression models e.g. [49].

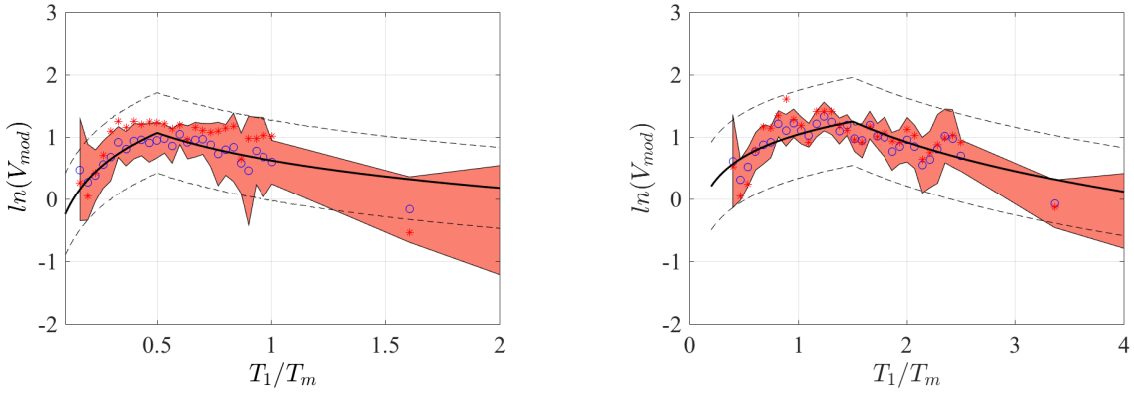

(a) 6-storey A1 building.

(b) 20-storey E1 building.

Figure 8: Mean base shear modification (V_{mod}) against period ratios (T_1/T_m), $q = 3$.

It is clear from Figure 8 that the relationship between inelastic shear demands and ground-motion frequency content is non-linear along the full range of period ratios. Besides, Figure 8a shows that in the short period range the base shear modification factor, V_{mod}, of mid-rise CLT structures (6-storey building) tends to increase with increasing period ratios up until $T_1/T_m = 0.5$. An inverse relationship is observed thereafter with decreasing V_{mod} values for longer periods, $T_1/T_m > 0.5$. The same piece-wise non-linear relationship is observed for the 20-storey building in Figure 8b, but in this case V_{mod} peaks at $T_1/T_m = 1.5$.

The influence of salient structural design parameters, namely, response modification factor, q, number of storeys, n, and the level of panel modularization, β, on the seismic strength demands in multi-storey CLT buildings is investigated in Figure 9. For this purpose, the evolution of base shear demands attained in CLT structures as a function of the behaviour factor, q, is illustrated in Figure 9a with reference to the 6-storey A1 building. This figure shows that the different trends observed before for the short ($T_1/T_m < 0.5$) and long period ranges ($T_1/T_m > 0.5$) persist regardless of the q-factor employed in the design. Although the rate of decay in V_{mod} at longer periods increases with increasing levels of assumed energy dissipation, q. The main feature of Figure 9a is that peak base shear ratios (V_{mod} at $T_1/T_m = 0.5$) increase in direct proportion to the q values, or what is the same, in direct proportion to the energy dissipation capacity of the building. This is reasonable as larger forces, relative to the corresponding yield values, are expected for higher ductility levels in strongly hardening structures like these.

The relationship between mean values of base shear demands, V_{mod}, and period ratios, T_1/T_m, for various joint density parameters, β, is presented in Figure 9b. It is clear from this figure that the mean base shear modification factor decreases with increasing levels of panel fragmentation, showing that a higher modularization level of CLT panels leads to lower shear demands. This is a reflection of the enhanced energy dissipation capacity associated with multiple rocking segments coupled with the more pronounced post-yield hardening effects of long CLT panels.

Finally, Figure 9c explores the relationship between base shear modification factor, V_{mod}, and the period ratio, T_1/T_m, for different building heights. The response of CLT building models of different number of storeys (i.e. n = {6,8,12,16,20}) but with a single line of vertical joinery (i.e. m = 1) designed with $q = 3$ is presented. It can be appreciated from Figure 9c that the mean base shear modification factor increases non-linearly with increasing period ratios irrespectively of the building height in the short period range, peaking at increasingly longer periods as the structures become taller (i.e. $T_1/T_m = \{0.5, 0.75, 1, 1.25, 1.5\}$).

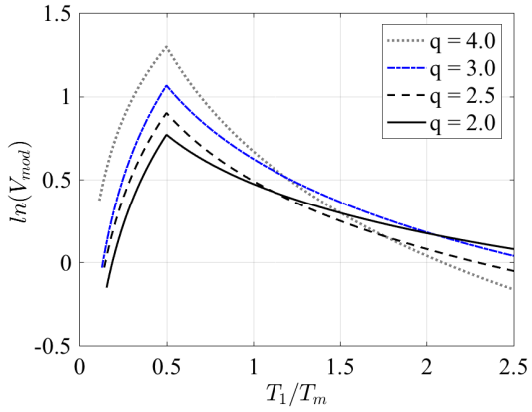

(a) Mean V_{mod} and T_1/T_m relationship for various behaviour factors (q) in 6-storey (A1) buildings.

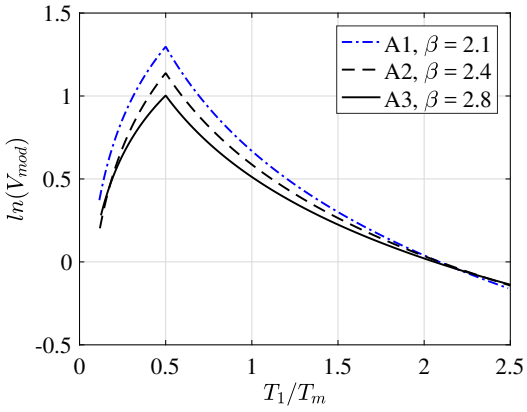

(b) Mean V_{mod} and T_1/T_m relationship for various joint density parameters (β) in 6-storey (A1) buildings, $q = 3$.

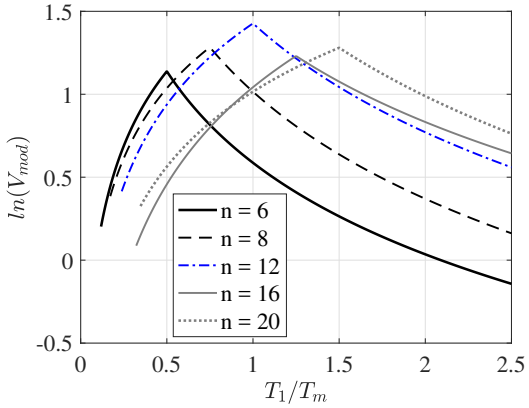

(c) Mean V_{mod} and T_1/T_m relationship for various building heights, $q = 3$.

Figure 9: Mean base shear modification (V_{mod}) against period ratios (T_1/T_m), for different structural parameters.

This observation hints to the central role played by resonance with the first building mode in the evaluation of shear demands. Furthermore, the largest base shear modification factors take place in buildings of around 12 storeys which fundamental period coincides with the mean period of the building (i.e. $T_1/T_m = 1$).

4.3. Inter-storey shear demands

A similar procedure as the one described above was followed to study the relationship between the inter-storey shear modification factors, $V_{st,mod}$, and the structural parameters of interest. Figure 10a shows the variation of $V_{st,mod}$ for the A1 (n = 6) building configuration as a function of the period ratio, T_1/T_m, while Figure 10b depicts the results corresponding to the E1 (n = 20) building. As before, the shaded regions in these figures represent the 95% confidence interval in the estimate of the mean storey shear modification factor. The dashed lines indicate the ± one standard deviation of the mean logarithmic storey shear modification factor, represented by the solid line. And the open circles (o) and asterisk (*) symbols denote the mean and median values within data bins, respectively.

It is clear from Figure 10 that, unlike the base shear modification factor, milder variations of $V_{st,mod}$ are expected for the long period range, especially in taller CLT buildings. It should be noted that a com-

plete lack of correlation between $V_{st,mod}$ and T_1/T_m at long periods is strictly valid only for taller building configurations (i.e. $n = \{16, 20\}$) with the lowest number of vertical joints, $m = 1$. If more vertical joints are employed (e.g. $m = 2$ or 3 corresponding to β values in the order of 3 or 3.4), or shorter structures are considered, the evolution of storey shear modification factors is mildly non-linear, as will be discussed below with reference to Figure 11c.

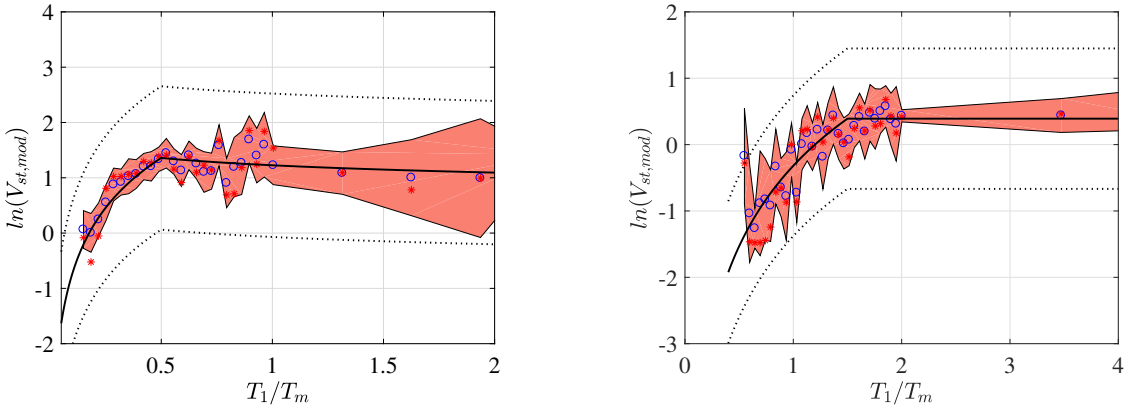

(a) 6-storey A1 building.

(b) 20-storey E1 building.

Figure 10: Mean storey shear modification factor ($V_{st,mod}$) against period ratios (T_1/T_m), for a behaviour factor of $q = 3$.

The effect of key structural parameters such as behaviour factor, q, number of storeys, n, and panel fragmentation, β, on the inter-storey seismic shear demands in CLT buildings is presented in Figure 11. Figure 11a displays the variation in mean storey shear modification factor ($V_{st,mod}$) as a function of the period ratio (T_1/T_m) for the D1 (n = 16) building configuration with the lowest panel fragmentation level and for various design response modification factors (i.e. $q = \{2, 2.5, 3, 4\}$). It can be appreciated from this figure that larger response modification factors, q, are associated with correspondingly larger inter-storey shear demand ratios, $V_{st,mod}$, along the full period range. Again, the significant levels of post-yield hardening experienced by tied down CLT panels can explain these tendencies. In general, short period structures will experience inelastic inter-storey shear demands at or below the ultimate forces predicted from a pushover analysis. On the other hand, in the long period range, $T_1/T_m \geq 1.2$, the inter-storey shear demands from non-linear response history analyses will exceed the non-linear static predictions except when q-factors of 2 or less are employed.

Similarly, the influence of panel fragmentation on the inter-storey shear demands is depicted in Figure 11b for A1, A2 and A3 ($n = 6$) building configurations. It can be observed from this figure that $V_{st,mod}$ decreases with increasing number of vertical joint lines, or higher β values. This can be attributed to the overall increment in energy dissipation capacity brought about by the larger number of ductile connectors. A change from $\beta = 2.5$ to $\beta = 3.6$, equivalent to going from a single vertical joint per wall to three vertical joints, reduces the shear demands in over 250% (note the logarithmic scale).

Finally, the relationship between the storey shear modification factor, $V_{st,mod}$, and the period ratio, T_1/T_m, for different building heights, n, is presented in Figure 11c. The buildings with the highest level of panel fragmentation studied (i.e. $m = 3$) are shown in this figure. It can be seen from Figure 11c that while lower shear demands are expected in the short period range for taller structures, larger shear demands will take place in the long period range in taller buildings. This can be attributed to the importance of higher mode-effects in the seismic response of buildings which becomes more prominent in taller, more slender, structures.

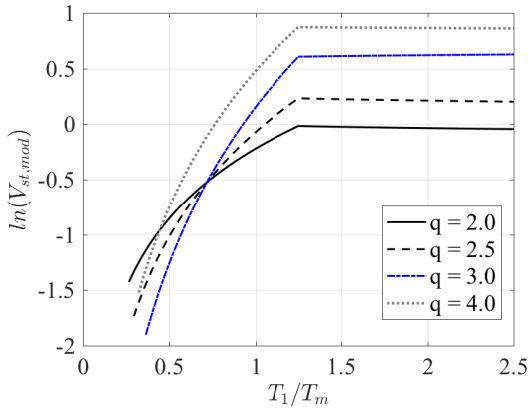

(a) Mean $V_{st,mod}$ and T_1/T_m relationship for various behaviour factors (q) in the 16-storey (D1) building.

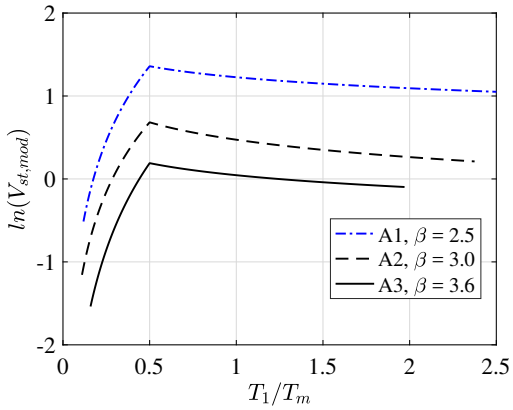

(b) Mean $V_{st,mod}$ and T_1/T_m relationship for various joint density parameters (β) in the 16-storey building, $q = 3$.

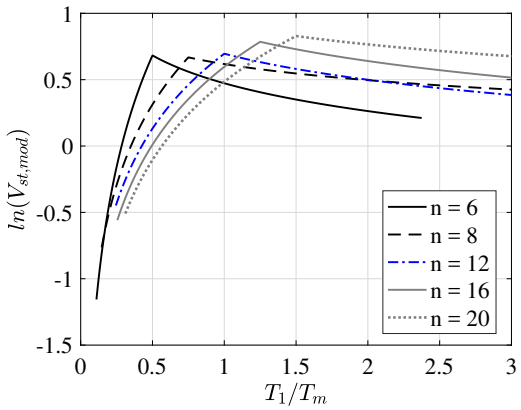

(c) Mean $V_{st,mod}$ and T_1/T_m relationship for various building heights (n), $q = 3$.

Figure 11: Mean storey shear modification ($V_{st,mod}$) against period ratios (T_1/T_m), for different key structural parameters.

5. Assessment of floor acceleration demands

5.1. Assessment procedure

As with shear forces, the extensive results from non-linear dynamic analyses carried out were employed to identify the main scaling trends in the acceleration response of CLT buildings. To undertake these analyses, the acceleration amplification factor, γ, was calculated as the ratio of the maximum floor acceleration, α_{max}, along the building height obtained from the non-linear response history analysis versus the spectral acceleration of the ground-motion corresponding to the fundamental vibration mode of the building, $S_a(T_1)$:

$$\gamma = \frac{\alpha_{max}}{S_a(T_1)} \tag{4}$$

It should be noted that, although some previous studies have used the ratio between the floor accelerations and the peak ground accelerations, α_{max}/PGA, as an amplification factor, the use of $S_a(T_1)$ instead of PGA is preferred since it generally leads to lower dispersion levels. A more comprehensive discussion on alternative earthquake intensity measures and their influence on the presentation of acceleration data can be found in

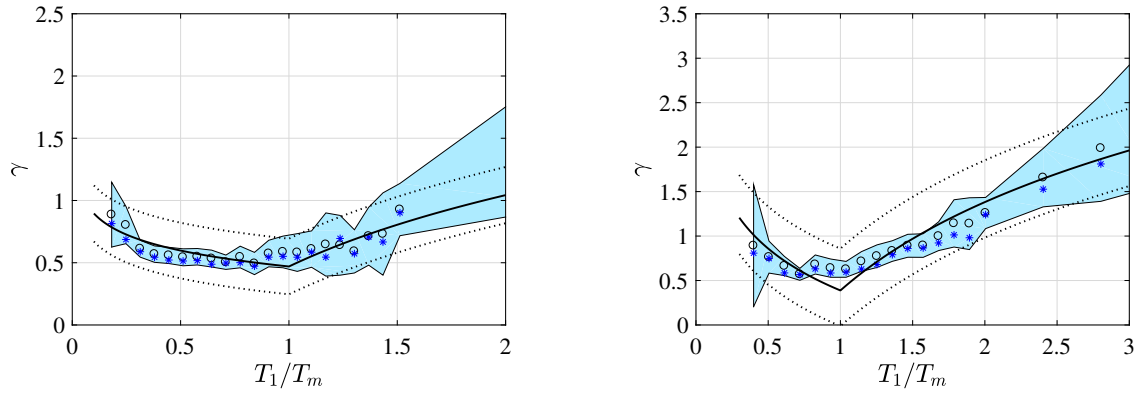

(a) 6-storey A1 building.

(b) 20-storey E1 building.

Figure 12: Mean peak floor acceleration amplification factor (γ) against period ratios (T_1/T_m), $q = 3$.

[46]. The next section discusses the influence of different parameters in the scaling of γ as defined in Equation 4. The main trends identified therein will be subsequently employed in latter sections of this paper to develop predictive models suitable for practical application.

5.2. Peak floor accelerations

The relationship between the acceleration amplification factor, γ, and the period ratio, T_1/T_m, is presented in Figure 12. Results are shown for two buildings, of 6 and 20 storeys, both with a single vertical joint per wall (i.e. $m = 1$) . The shaded area in these figures show the 95% confidence interval in the estimate of mean while open circles (o) and asterisk (*) symbols denote the individual bin mean and median values, respectively. Likewise, the dashed lines indicate $\pm$ 1 standard deviation of the mean amplification of peak acceleration demands for the non-linear model fitted to the data. The mean γ estimated by the fitted model is depicted as a solid line in Figure 12.

Figure 12 demonstrates the importance of taking into account the frequency content of the ground-motion, characterised herein by its mean period, T_m, when evaluating inelastic demands. Two clear behavioural regions are identified in Figure 12 depending on whether $T_1/T_m < 1$ or $T_1/T_m > 1$. Regardless of the building height, acceleration amplification demands decreases with increasing period ratios in the short period range ($T_1/T_m < 1$), reaching a minimum at $T_1 = T_m$, and increasing thereafter for longer periods. The response in the short period range, can be explained by the period lengthening associated with a plastic response coupled with the inherent scaling of the ground-motion spectral ordinates in this region. On the other hand, the increasing amplification of accelerations observed for $T_1 > T_m$ is a clear manifestation of the higher mode effects and emphasize the adequacy of T_m as a scalar frequency content indicator.

The effect of the behaviour factor, q, on γ is investigated in Figure 13a. This figure shows the relationship between peak floor acceleration factors and period ratios, T_1/T_m, for various behaviour factors (i.e. $q = \{2, 2.5, 3, 4\}$). It is clear from Figure 13a that lower design behaviour factors are associated with lower acceleration levels when $T_1 > T_m$. Conversely, the effects of the behaviour factor are negligible for $T_1 < T_m$. This reinforces the previous observations regarding the importance of higher mode effects in the long period range and the mitigation of peak accelerations associated with the period lengthening which, as expected, is more pronounced when more inelastic behaviour takes place.

On the other hand, the level of panel fragmentation, characterized by β, is noticeable but less important. This can be appreciated in Figure 13b which summarizes the distribution of acceleration amplification factors, γ, in 6-storey building models with different wall arrangements conductive to β values of

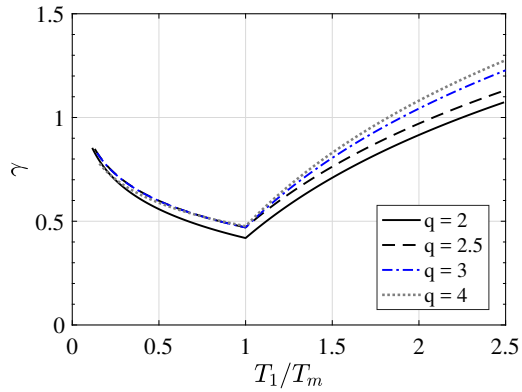

(a) Mean γ and T_1/T_m relationship for various behaviour factors (q) in the 6-storey building.

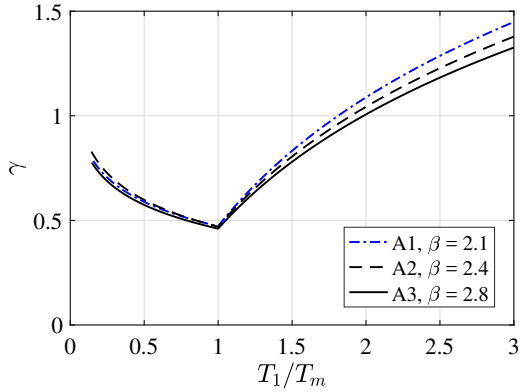

(b) Mean γ and T_1/T_m relationship for various joint density parameters (β) in the 6-storey building, $q = 3$.

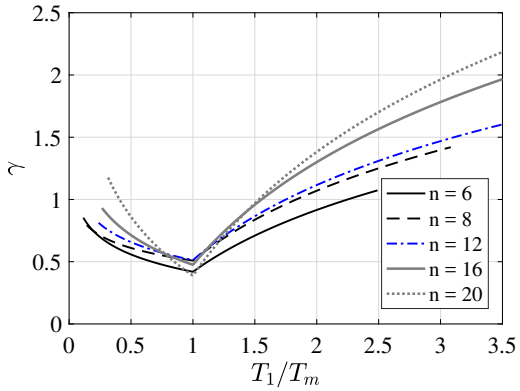

(c) Mean γ and T_1/T_m relationship for various building heights (n), $q = 3$.

Figure 13: Mean storey shear modification (γ) against period ratios (T_1/T_m), for different key structural parameters.

$\beta = \{2.1, 2.4, 2.8\}$ representing 1, 2 and 3 vertical joints per wall, respectively. Again, the mitigating effects of higher levels of non-linear response in peak accelerations are evident from Figure 13b where higher β values (higher energy dissipation capacities) are associated with lower γ factors.

Likewise, Figure 13c offers an additional confirmation of the importance of higher mode effects on the determination of peak floor acceleration demands. The figure compares mean amplification factors of acceleration demands in buildings of different heights ($n = \{6, 8, 12, 16, 20\}$ storeys) for a given number of vertical joint lines ($m = 1$). The same two spectral regions identified above are observed for all building heights in Figure 13c with higher mean accelerations occurring in taller buildings.

6. Predictive models

Non-linear regression models for the estimation of base shears, inter-storey shears and floor accelerations are developed and discussed in this section. These models are constructed on the basis of the extensive numerical analyses presented in previous sections of this paper. To this end, standard regression procedures were followed to identify the most appropriate expressions. Whenever possible, model simplifications were implemented in order to strike a balance between prediction accuracy and complexity of formulation.

6.1. Base shear modification factor

The following equation was developed by taking into consideration the parameters that have the greatest influence on the base shear modification factor and their interrelations as described above:

$$lnV_{mod} = a + b \cdot \lambda + (c + d \cdot q) \cdot ln\left[min\left(\frac{T_1}{T_m}, \xi\right)\right] + e \cdot ln\left[max\left(\frac{T_1}{T_m}, \xi\right)\right] + f \cdot \beta + g \cdot \alpha \quad (5)$$

where V_{mod} is the base shear modification factor, λ is the building aspect ratio which correlates with the number of storeys, q is the design behaviour factor, T_1/T_m is the period ratio, β is the joint density parameter, α is the plasticity resistance ratio, ξ is the building height index, and a, b, c, d, e, f, g are regression coefficients. The assumption of log-normality was verified during preliminary analyses [20]. The building height index, ξ, which controls the period associated which maximum shear forces is obtained from:

$$\xi = 3.42 \times 10^{-4}(n)^3 - 1.48 \times 10^{-2}(n)^2 + 2.65 \times 10^{-1}(n) - 6.23 \times 10^{-1} \quad (6)$$

where n represents the number of storeys. Table 5 presents the computation of building height indexes obtained from Equation 6, and employed in the models, while Table 6 summarizes the regression coefficients associated with Equation 5. The standard deviation associated with this model is $\sigma = 0.77$. These coefficients were obtained by means of a generalized non-linear least squares algorithm and were found to be statistically significant in all cases. A residual plot of the parameters that are used in the predictive model is presented in Figure 14. It is clear from this plot that the model is able to explain all significant trends in the data and no residual heteroskedasticity was identified.

6.2. Inter-storey shear modification factor

A similar prediction model was employed to estimate the storey shear modification factor as a function of the key structural parameters such as λ, q, T_1/T_m, β, and α as described in the previous section. This functional form is indicated in Equation 7:

$$lnV_{st,mod} = a + b \cdot \lambda + (c + d \cdot q) \cdot ln\left[min\left(\frac{T_1}{T_m}, \xi\right)\right] + e \cdot ln\left[max\left(\frac{T_1}{T_m}, \xi\right)\right] + f \cdot \beta + g \cdot \alpha \quad (7)$$

As per above, all regression terms were found to be statistically significant and are presented in Table 7. The standard deviation associated with this model is $\sigma = 1.15$. Finally, the residuals of the parameters used in the predictive model are presented in Figure 15. As with base shear modification factor, there is no significant trend or heteroskedasticity observed in the residual plots.

It is clear from Figures 8 and 10 that the models associated with Equations 5 and 7 perform well. It should be recalled that the solid lines in these figures represent the fitted model whereas the associated $\pm$one standard deviation curves are indicated with the dotted lines. Despite their relatively simple form, the models proposed are robust and estimate well the main scaling features of shear demands along the full range of periods and for all building configurations.

Table 5: Building height indexes (ξ) computed by means of Equation 6.

n	6	8	12	16	20
ξ	0.5	0.75	1.00	1.25	1.50

Table 6: Regression coefficients for the base shear modification factor (V_{mod}) in Equation 5

a	b	c	d	e	f	g
2.1169	0.1205	0.2150	0.1315	-0.7906	-0.2269	-0.3678

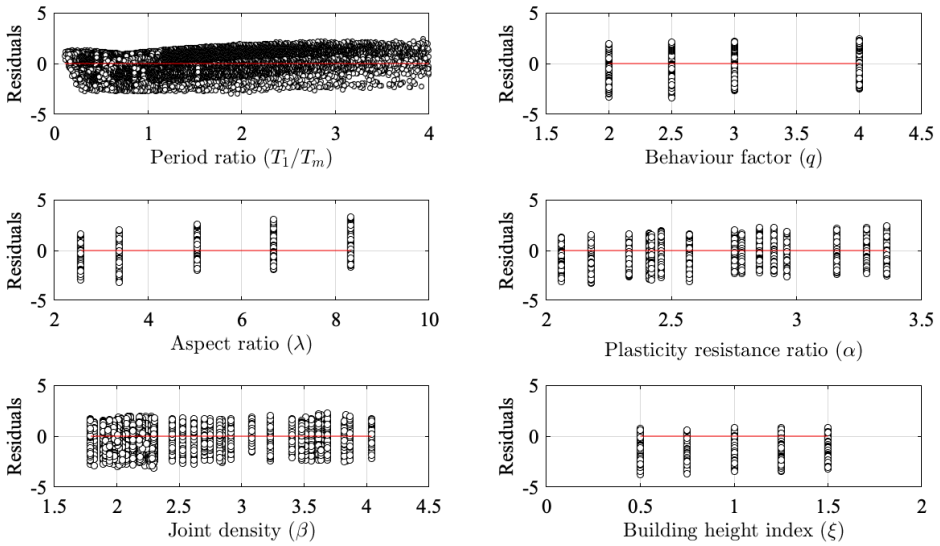

Figure 14: Residual plots associated with the base shear modification factor (V_{mod}) prediction model.

Table 7: Regression coefficients for the storey shear modification factor ($V_{st,mod}$) in Equation 7.

a	b	c	d	e	f	g
3.7369	-0.1567	0.7733	0.1410	-0.0339	-0.3317	-0.5105

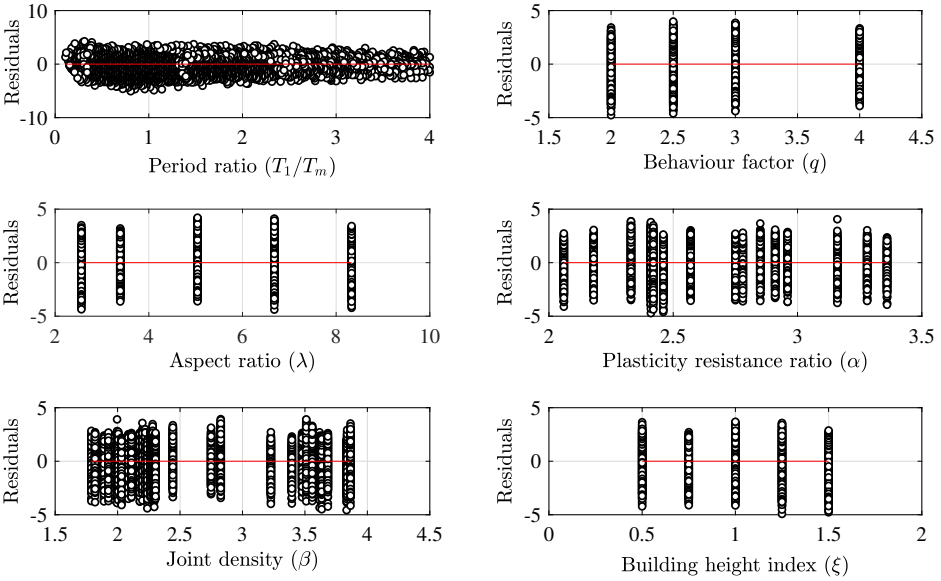

Figure 15: Residual plots associated with the storey shear modification factor $V_{st,mod}$ prediction model.

6.3. Model simplifications

A number of simplifications can be implemented in the models described above. In particular, the equations for height index, ξ, and storey shear modification factor, $V_{st,mod}$, presented in the previous section can be simplified without jeopardizing the model's accuracy for practical purposes. These simplifications are detailed and assessed below.

Building height index

The number of terms required for the computation of the building height can be reduced by linearising Equation 6. Therefore, the following equation can be derived:

$$\xi_S = 0.0686 \cdot n + 0.1494 \tag{8}$$

Table 8 presents a comparison of the computed building height indexes (ξ and ξ_S) associated with Equations 6 and 8. It can be appreciated from Table 8 that the simplified model function is able to approximate Equation 6 with an error of less than 12%.

Storey shear modification factor

Since the non-linear correlation between the storey shear modification factor, $V_{st,mod}$, and the period ratio, T_1/T_m, in the long period range was found to be small or negligible, a simplified functional form with a reduced number of terms can be proposed as follows:

$$lnV_{st,mod} = a + b \cdot ln\left[min\left(\frac{T_1}{T_m}, \xi\right)\right] \tag{9}$$

The regression coefficients for the simplified model is presented in Table 9.

Figures 16a and 16b show the performance, against the observed response, of the new formulation for A1 (n = 6) and E1 (n = 20) building configurations, respectively. It is apparent from these figures that the plateau of the simplified model (Equation 9) is able to reproduce the tendency and variabilities of the building response. An alternative comparison between the median estimations of the full and simplified models associated with Equations 7 and 9 is offered in Figure 17. It can be appreciated from this figure that while an almost perfect match is observed for the 20-storey building, a maximum divergence in the $\ln(V_{st,mod})$ in the order of 10% is attained in the 6-storey building at the longest period ratio. The acceptance of this degree of over-conservativeness in storey shear estimations for low and medium-rise CLT buildings ought to be assessed in a case by case basis.

Table 8: Comparison of building height indexes, ξ, obtained with Equations 6 and 8.

n	6	8	12	16	20
ξ	0.5	0.75	1.00	1.25	1.50
ξ_S	0.56	0.70	0.97	1.25	1.52
Error %	12	6.7	3.0	0.0	1.3

Table 9: Regression coefficients for the storey shear modification factor ($V_{st,mod}$), obtained with the simplified Equation 9.

a	b
-1.8110	0.4028

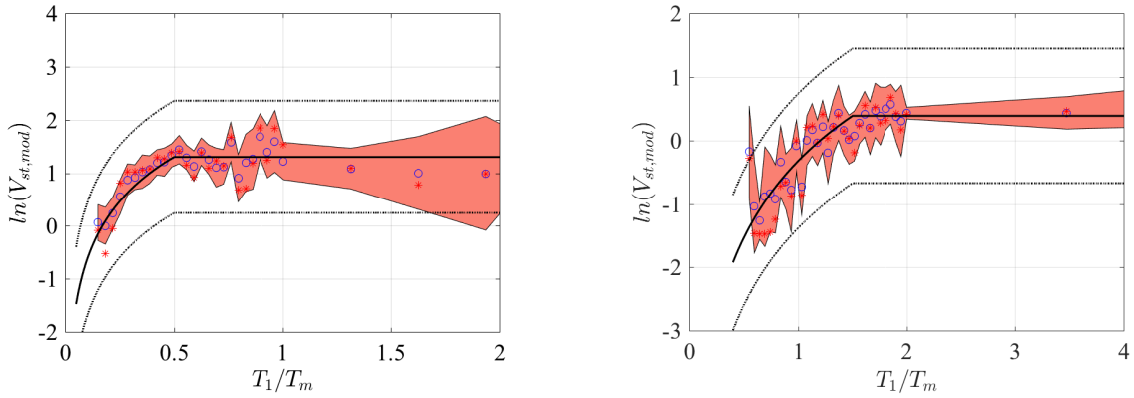

(a) 6-storey A1 building. (b) 20-storey E1 building.

Figure 16: Mean storey shear modification ($V_{st,mod}$) against period ratios (T_1/T_m), obtained using the simplified prediction model of Equation 9, for a response modification factor of $q = 3$.

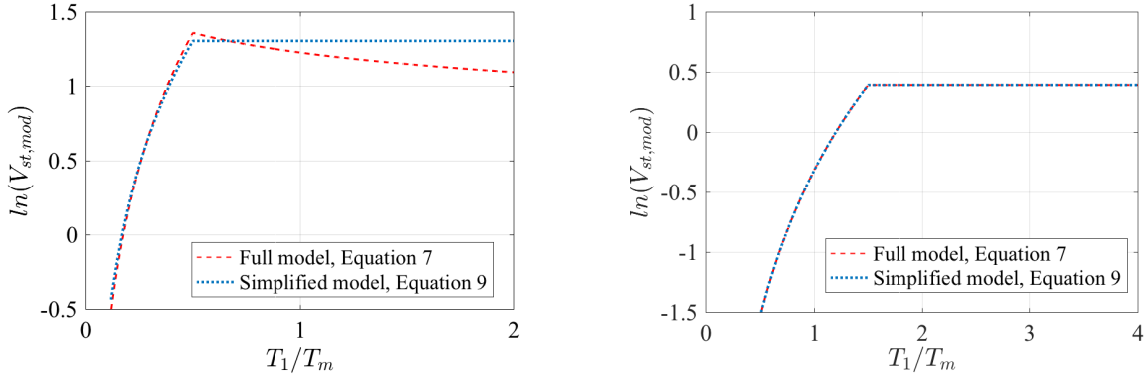

(a) 6-storey A1 building. (b) 20-storey E1 building.

Figure 17: Comparison between the results of mean storey shear modification ($V_{st,mod}$) against period ratios (T_1/T_m), obtained by means of the full and simplified models for a response modification factor of $q = 3$.

6.4. Peak floor acceleration factor

A predictive model was developed to estimate seismic acceleration demands in multi-storey CLT buildings by means of general statistical procedures. On the basis of preliminary parametric investigations, the joint density, β, design behaviour factor, q, and the period ratio, T_1/T_m, were found to have non-negligible influence on the seismic acceleration demands experienced by CLT buildings. In line with this, the best-fit regression model described by Equation 10 is proposed herein. To this end, Table 10 summarizes the regression coefficients obtained by robust non-linear regression employing the functional form presented in Equation 10. All coefficients were tested for statistical significance. The standard deviation associated with this model is $\sigma = 0.41$. Also, Figure 18 shows the corresponding residual plots. It can be seen that no significant residual trend can be identified, suggesting that the model is able to explain the main trends of the acceleration response in CLT buildings, lending further support to the regression function employed.

$$\gamma = a \cdot \beta + b \cdot q \cdot ln\left[\min\left(\frac{T_1}{T_m}, 1\right)\right] + c \cdot ln\left[\max\left(\frac{T_1}{T_m}, 1\right)\right] \tag{10}$$

Table 10: Regression coefficients for the peak floor acceleration (γ) in Equation 10.

a	b	c
0.4112	-0.0775	-0.0929

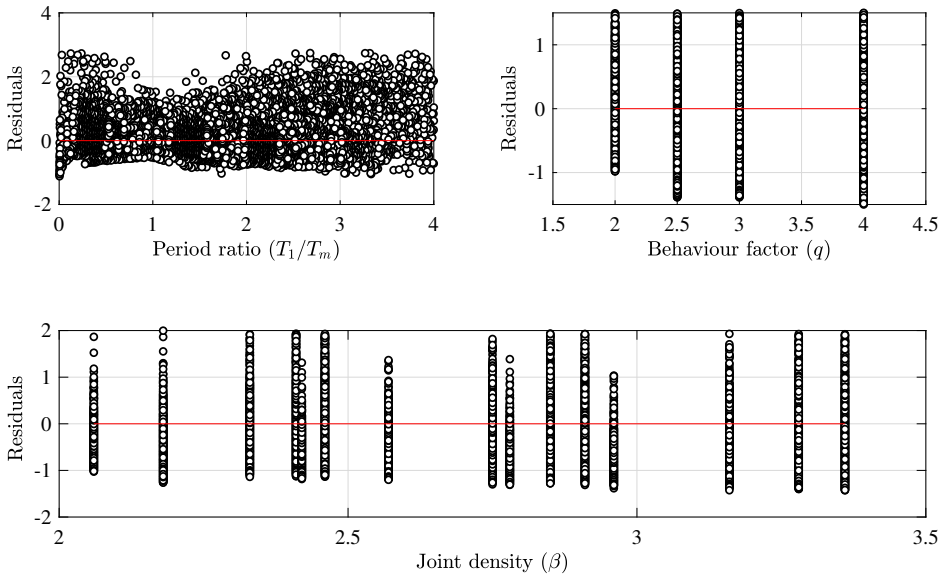

Figure 18: Residual plots associated with the acceleration amplification factor (γ) prediction model.

Figure 12 shows the performance of the model (solid line) against the extensive dataset of non-linear responses generated in this study. The comparisons offered in Figure 12, although not predictive, offer some assurance on the abilities of the model to represent seismic acceleration demands in multi-storey CLT structures. It is also apparent from Figure 12 that the regression model is less well constrained for very long periods, which is a direct reflection of the higher mode effects on the accelerations at the upper floors of taller buildings. Importantly, the expression employed to define the model makes use of structural parameters of easy collection that do not require any prior analysis to be performed.

The expressions proposed above can be used for a first-level deterministic performance-based assessment of the structural response of CLT buildings. This will require the selection of a design earthquake scenario, defined by magnitude, distance and a number of standard deviations above the median. The mean period of the associated ground-motion can be estimated based on the ground-motion prediction equations proposed by Rathje *et al.* [43] or Du [50] which can include site conditions and directivity effects. Once T_m and the corresponding structural characteristics are defined, the base shear, inter-storey shear or peak floor acceleration models described above can be used to predict the corresponding median structural response. Alternatively, the number of standard deviations below or above the median estimate of the response parameter under consideration can be used for a first order approximation of the variability induced in the calculations given a specified earthquake intensity and site conditions.

7. Conclusions

This paper has examined the influence of key structural parameters and the ground-motion frequency content on the seismic strength and acceleration demands of multi-storey CLT structures. Maximum base shears, inter-storey shears and peak floor accelerations were studied and evaluated. For this purpose, a comprehensive database of two-dimensional advanced numerical models of CLT buildings was assembled and subjected to a large set of recorded ground-motions. It is thought that this paper is the first to undertake such a detailed parametric study on mid-rise and high-rise CLT building structures. The seismic demands were expressed in terms of base shear modification factors, V_{mod}, storey shear modification factors, $V_{st,mod}$, and peak floor acceleration amplification factors, γ. In all three cases, the seismic demands were found to exhibit a strong dependency on the mean period of the acceleration series, T_m, and distinct behavioural trends were identified for the short and long period ranges.

The relationships between base shear and inter-storey shear ratios and ground-motion frequency content were observed to be non-linear along the full range of period ratios, T_1/T_m, studied. These shear demands tend to increase with increasing period ratios up until a maximum value is reached, decreasing thereafter for longer periods. Moreover, maximum shear ratios were observed to increase in direct proportion to the energy dissipation capacity of the building, although these effects are larger for global shear demands than for inter-storey forces. In general, larger levels of plasticity (e.g. greater q factors) and higher degrees of panel fragmentation lead to lower relative shear demands. Alternatively, acceleration amplification demands decrease with increasing period ratios in the short period range ($T_1/T_m < 1$) and increase thereafter for increasing period ratios regardless of the building height. As with shear demands, higher degrees of CLT modularization are associated with lower acceleration amplification factors and higher mean accelerations occur in taller buildings due to higher mode effects. The findings of this study emphasize the efficiency of T_m as a scalar frequency content indicator. Finally, robust regression models were developed for the estimation of shear and acceleration demands in CLT buildings. These predictive expressions can provide guidance to designers for the implementation of adequate capacity design approaches and during the evaluation of potential seismic damage to non-structural elements and building contents in CLT structures.

Acknowledgements

The authors would like to thank the Imperial College London and Old Centralians' Trust for funding the doctoral studies of the first author. The technical support of the Research Computing Service at Imperial is also gratefully acknowledged.

References

[1] Ceccotti A, Sandhaas C, Okabe M, Yasumura M, Minowa C, and Kawai N. 2013. *SOFIE project - 3D shaking table test on a seven-storey full-scale cross-laminated timber building.* Earthquake Engineering and Structural Dynamics, 42:2003-2021.

[2] Ceccotti A, Lauriola MP, Pinna M, Sandhaas C. 2006b. *SOFIE project: cyclic tests on cross-laminated wooden panels.* In Proceedings of the 9th World Conference on Timber Engineering (WCTE), Portland, USA.

[3] Popovski M, Gavric I. 2015 *Performance of a 2-story CLT house subjected to lateral loads.* ASCE J Struct Eng. doi:10.1061/(ASCE)ST.1943-541X.0001315.

[4] Yasumura M, Kobayashi K, Okabe M, Miyake T, Matsumoto K. 2015. *Full-scale tests and numerical analysis of low-rise CLT structures under lateral loading.* ASCE J Struct Eng. doi:10.1061/(ASCE)ST.1943-541X.0001348.

[5] Flatscher G, Schickhofer G. 2015. *Shaking-table test of a cross-laminated timber structure.* Proc ICE Struct Build 168(11):878888. doi:10.1680/stbu.13.00086.

[6] Málaga-Chuquitaype C, Skinner J, Dowdall A, Kernohan J. 2016. *Response of CLT shear walls under cyclic loads.* World Conference on Timber Engineering, Vienna, Austria.

[7] Dujic B., Pucelj J., Zarnic R. 2004. Testing of Racking Behavior of Massive Wooden Wall Panels. Proceedings of the 37th CIB-W18 Meeting, paper 37-15-2, Edinburgh, Scotland

[8] Dujic B, Strus K, Zarnic R, Ceccotti A. 2010. *Prediction of dynamic response of a 7-storey massive XLam wooden building tested on a shaking table.* In: Proceedings of the 11th world conference on timber engineering WCTE, Riva del Garda, Italy.

[9] Gavric I, Fragiacomo M, Ceccotti A. 2015. *Cyclic behavior of CLT wall systems: Experimental tests and analytical prediction models.* Journal of Structural Engineering 141(11):04015034.
[10] Popovski, M. and Karacabeyli, E. 2012. *Seismic behaviour of cross-laminated timber structures.* In Proceedings of the 15th World Conference on Earthquake Engineering, Lisbon, Portugal.
[11] Pozza L, Scotta R, Trutalli D, Polastri A. 2015. *Behaviour factor for innovative massive timber shear walls.* Bulletin of Earthquake Engineering 13(11):3449-3469.
[12] Ceccotti A, Sandhaas C. 2010. *A proposal for a standard procedure to establish the seismic behaviour factor q of timber buildings.* World Conference on Timber Engineering.
[13] Fragiacomo M, Dujic B, Sustersic I. 2011. *Elastic and ductile design of multi-storey crosslam massive wooden buildings under seismic actions.* Eng Struct 33(11):3043-3053.
[14] Pei S, van de Lindt JW, Popovski M. 2013. *Approximate R-factor for cross-laminated timber walls in multistory buildings.* J Archit Eng 19(4):245-255.
[15] Popovski M, Pei S, van de Lindt JW, Karacabeyli E. 2014. *Force modification factors for CLT structures for NBCC.* Mater J Timber Struct 9:543-553.
[16] Rinaldin G, Fragiacomo M. 2016. *Non-linear simulation of shaking-table tests on 3- and 7-storey X-Lam timber buildings.* Eng Struct 113:133-148.
[17] ASCE .2016. *Minimum design loads for building and other structures.* Standard ASC/SEI 7-16, American Society of Civil Engineers, Reston, VA, USA.
[18] Sustersic I, Fragiacomo M, Dujic B. 2016. *Seismic analysis of crosslaminated multistorey timber buildings using linear and nonlinear static and dynamic methods.* ASCE J Struct Eng, Special issue on Seismic Resistant Timber Struct 2016;142(4), E4015012.
[19] Follesa M, Fragiacomo M, Casagrande D, Tomasi R, Piazza M, Vassallo D, Canetti D, Rossi S. 2018. *The new provisions for the seismic design of timber buildings in Europe.* Eng Struct 168:736-747.
[20] Demirci C, Málaga-Chuquitaype C, and Macorini L. 2018. *Seismic drift demands in multi-storey cross-laminated timber buildings.* Earthquake Engineering & Structural Dynamics. 47:1014-1031.
[21] Chopra A, Chintanapakdee C. 2001. *Comparing response of sdf systems to near-fault and far-fault earthquake motions in the context of spectral regions.* Earthquake Engineering and Structural Dynamics. 30(12):1769-1798.
[22] Demirci C, Málaga-Chuquitaype C, and Macorini L. 2017. *Seismic behaviour and Design of Tall Cross Laminated Timber Buildings.* Proc. of the 16th World Conference on Earthquake Engineering, Santiago, Chile.
[23] Málaga-Chuquitaype, C, Elghazouli, A. 2016. *Chapter 8: Design of timber structures.* In Seismic Design to Eurocode 8.
[24] BS EN 14081-1:2005. *Timber structures. Strength graded structural timber with rectangular cross section. General requirements.* ISBN: 978 0 580 71689 8.
[25] European Committee for Standardization (CEN). 2004. *Eurocode 8: Design of structures for earthquake resistance-Part 1: General rules, seismic actions and rules for buildings..* EN 1998-1. Brussels, Belgium.
[26] European Committee for Standardization (CEN). 2004. *Eurocode 1: Actions on structures.* BS EN 1991-1-1. Brussels, Belgium.
[27] Jorissen A, Fragiacomo M. 2011. *General notes on ductility in timber structures.* Engineering structures, 33(11), 2987-2997.
[28] Gavric I, Fragiacomo M, Ceccotti A. 2013. *Capacity seismic design of X-LAM wall systems based on connection mechanical properties.* In Meeting forty-six of the Working Commission W18-Timber Structures, CIB, International Council for Research and Innovation (pp. 285-298). Timber Scientific Publishing-KIT Holzbau und Baukonstruktionen.
[29] Blass HJ, Uibel T. 2007. Tragfhigkeit von stiftfrmigen Verbindungsmitteln in Brettsperrholz in opus.bibliothek.fh-aachen.de
[30] Casagrande D, Sartori T, Tomasi R. 2014. *Capacity design approach for multi-storey timber-frame buildings.* In: Proc. of the international network on timber engineering research meeting INTER, Bath, United Kingdom, paper 4715-3.
[31] Rotho Blaas S.r.l. 2018. Pilastre e connettori per legno. Cortaccia, BZ, Italy.
[32] Sustersic I, Fragiacomo M, and Dujic B. 2015. *Seismic Analysis of Cross-Laminated Multistory Timber Buildings Using Code-Prescribed Methods: Influence of Panel Size, Connection Ductility, and Schematization.* Journal of Structural Engineering, 10.1061/(ASCE)ST.1943-541X.0001344, E4015012.
[33] Ceccotti A. 2008. *New technologies for construction of medium-rise buildings in seismic regions: The XLAM case.* Structural Engineering International. 18(2): 156-165.
[34] Pozza L, Trutalli D. 2017. *An analytical formulation of q-factor for mid-rise CLT buildings based on parametric numerical analyses.* Bulletin of Earthquake Engineering. 15:2015-2033.
[35] R Core Team. 2013. R: A language and environment for statistical computing. R Foundation for Statistical Computing, Vienna, Austria. URL http://www.R-project.org/.
[36] Demirci C. 2018. How to modify a correlation matrix plot? URL https://stackoverflow.com/questions/15271103/how-to-modify-this-correlation-matrix-plot/48662697#48662697
[37] McKenna, F. 2011. *OpenSees: A Framework for Earthquake Engineering Simulation.* Computing in Science and Engg. 13(4): 58-66.
[38] Rinaldin, G, Amadio, C, Fragiacomo, M. 2013. *A component approach for the hysteretic behaviour of connections in cross-laminated wooden structures.* Earthquake engineering and structural dynamics. 42(13): 2023-2042.
[39] Gavric I, Fragiacomo M, Ceccotti A. 2015. *Cyclic behaviour of typical metal connectors for cross-laminated (CLT) structures.* Materials and Structures. 48:1841-1857. DOI 10.1617/s11527-014-0278-7.
[40] Gavric I, Fragiacomo M, Ceccotti A. 2015. *Cyclic behavior of typical screwed connections for cross-laminated (CLT) structures.* Eur. J. Wood Prod. 73:179-191. DOI 10.1007/s00107-014-0877-6.
[41] Hancock J, Bommer J, Stafford, P. 2008. *Numbers of scaled and matched accelerograms required for inelastic dynamic*

analyses. Earthquake Engineering and Structural Dynamics 37(14):1585-1607.

[42] Rathje EM, Abrahamson NA, Bray JD. 1998. *Simplified frequency content estimates of earthquake ground motions.* J Geotech Geoenviron Eng. 124(2):150-9.

[43] Rathje EM, Faraj F, Russel S, Bray JD. 2004. *Empirical relationships for frequency content parameters of earthquake ground motions.* Earthq Spectra. 20(1):119-44.

[44] Málaga-Chuquitaype C. 2015. *Estimation of peak displacements in steel structures through dimensional analysis and the efficiency of alternative ground-motion time and length scales.* Engineering Structures. 101:264-278.

[45] Málaga-Chuquitaype C, Bougatsas K. 2017. *Vector-IM-based assessment of alternative framing systems under bi-directional ground-motion.* Engineering Structures. 132:188-204.

[46] Málaga-Chuquitaype C, Psaltakis ME, Kampas G, Wu J. 2019. *Dimensionless fragility analysis of seismic acceleration demands through low-order building models.* Bulletin of Earthquake Engineering. https://doi.org/10.1007/s10518-019-00615-2

[47] Imperial College High Performance Computing Service, doi: 10.14469/hpc/2232.

[48] Sanchez-Ricart L, Plumier A. 2008. *Parametric study of ductile moment-resisting steel frames: A first step towards Eurocode 8 calibration.* Earthquake Engineering and Structural Dynamics. 37:11351155.

[49] Stafford P, Mendis R, Bommer J. 2008. *Dependence of damping correction factors for response spectra duration and number of cycles.* Journal of Structural Engineering, ASCE, 134: 1364-1373

[50] Du W. 2017. *An empirical model for the mean period (Tm) of ground motions using the NGA-West2 database.* Bulletin of Earthquake Engineering, 15 (7):2673 -2693